

Multifunctional Nanoplatfrom-Mediated Chemo-Photothermal Therapy Combines Immunogenic Cell Death with Checkpoint Blockade to Combat Triple-Negative Breast Cancer and Distant Metastasis

Hui Zhu ^{1,2}, Ke Yang³, Huan Yao¹, Xueying Chen¹, Shujin Yan ^{1,2}, Yiman He^{1,2}, Yang Cao², Jie Luo¹, Dong Wang¹

¹Department of Ultrasound, The First Affiliated Hospital of Chongqing Medical University, Chongqing, People's Republic of China; ²Chongqing Key Laboratory of Ultrasound Molecular Imaging, Chongqing Medical University, Chongqing, People's Republic of China; ³Pediatric Research Institute, Children's Hospital of Chongqing Medical University, Chongqing, People's Republic of China

Correspondence: Jie Luo; Dong Wang, Department of Ultrasound, The First Affiliated Hospital of Chongqing Medical University, 1 Youyi Road, Yuzhong District, Chongqing, 400042, People's Republic of China, Email luojie1983@cqmu.edu.cn; wangdong4429@cqmu.edu.cn

Background: Breast cancer has become the most common cancer in women. Compare with other subtypes of breast cancer, triple-negative breast cancer (TNBC) is more likely to relapse and metastasize. Highly effective therapeutic strategies are desperately needed to be explored. In this study, a multifunctional nanoplatfrom is expected to mediate chemo-photothermal therapy, which can combine immunogenic cell death with checkpoint blockade to combat TNBC and distant metastasis.

Methods: Poly (lactic acid-glycolic acid)-Poly (ethylene glycol) (PLGA-PEG) nanoparticles (NPs), a type of polymeric NPs, loaded with IR780, a near-infrared (NIR) dye, and doxorubicin (DOX) as the chemotherapeutic drug, were assembled by an improved double emulsification method (designated as IDNPs). The characterization, intracellular uptake, biosafety, photoacoustic (PA) imaging performance, and biodistribution of IDNPs were studied. Chemo-photothermal therapeutic effect and immunogenic cell death (ICD) were evaluated both in vitro and in vivo. The potency of chemo-photothermal therapy-triggered ICD in combination with anti-PD-1 immune checkpoint blockade (ICB) immunotherapy in eliciting immune response and treating distant tumors was further investigated.

Results: IR780 and DOX were successfully loaded into PLGA-PEG to form the IDNPs, with size of 243.87nm and Zeta potential of -6.25mV. The encapsulation efficiency of IR780 and DOX was 83.44% and 5.98%, respectively. IDNPs demonstrated remarkable on-site accumulation and PA imaging capability toward 4T1 TNBC models. Chemo-photothermal therapy demonstrated satisfactory therapeutic effects both in vitro and in vivo, and triggered ICD efficiently. ICD, in combination with anti-PD-1, provoked a systemic antitumor immune response against distant tumors.

Conclusion: Multifunctional IDNPs were successfully synthesized to mediate chemo-photothermal therapy, which combines immunogenic cell death with checkpoint blockade to combat TNBC and distant metastasis, showing great promise preclinically and clinically.

Keywords: immunogenic cell death, immunotherapy, checkpoint blockade, chemo-photothermal therapy, triple-negative breast cancer

Introduction

According to the International Agency for Research on Cancer, breast cancer has overtaken lung cancer to become the most common cancer among women.¹ Compare to other subtypes of breast cancer, triple-negative breast cancer (TNBC) is more likely to relapse and metastasize.²⁻⁴ Current mainstream treatments include surgery removal, radiotherapy, chemotherapy, and endocrine therapy.⁵⁻¹⁰ However, the inhibitory effects of monotherapy on TNBC are limited.¹¹

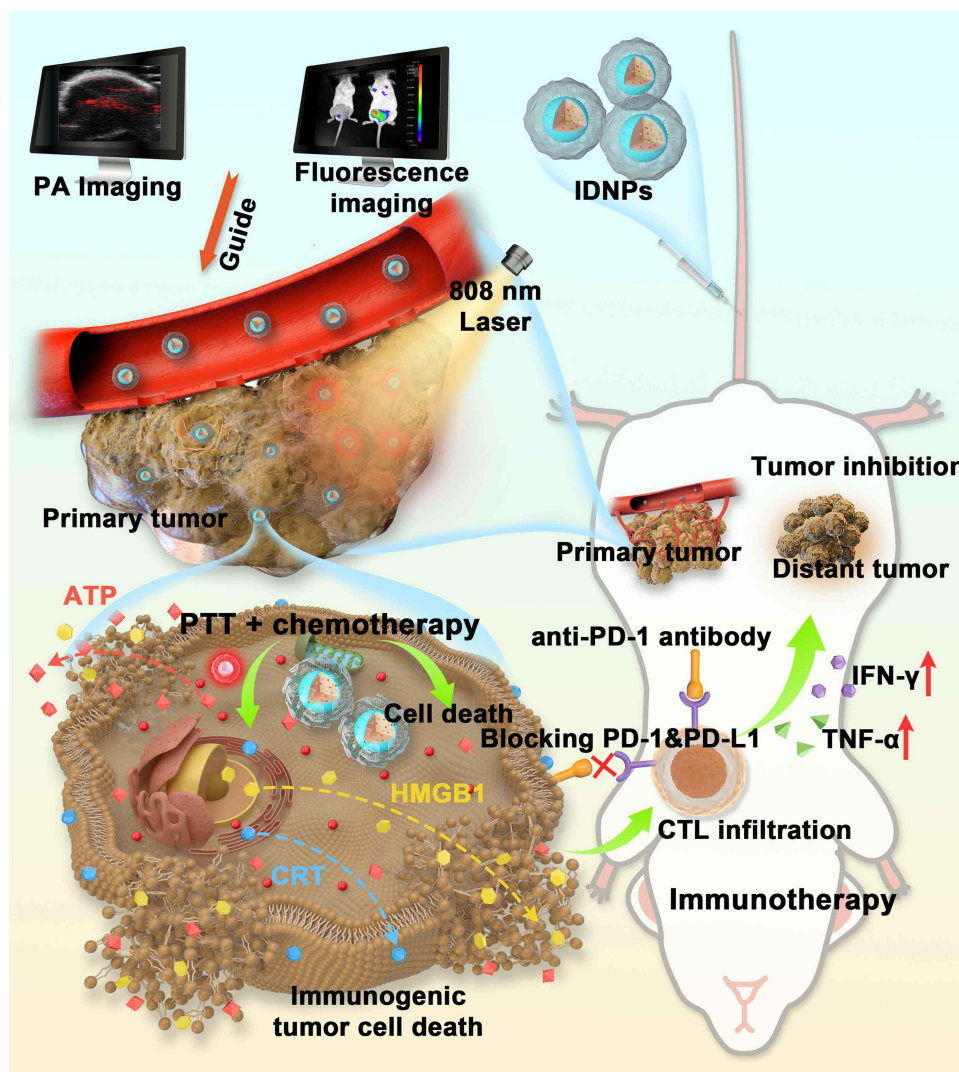
Among emerging therapeutic modalities, photothermal therapy (PTT), as a minimally invasive therapeutic strategy, has been extensively explored to treat breast cancer, which presented fairly high effectiveness.^{12,13} Typically, PTT is achieved by local hyperthermia caused by the thermal energy from the photosensitizer's conversion of a near-infrared (NIR) light energy, inducing damage to tumor cells.^{5,14–16} Nevertheless, in the consideration of the limited tissue penetration of NIR light, inevitably, not all tumor cells can be irradiated in a relatively large tumor mass, resulting in recurrence after PTT. It has been reported that chemotherapy can compensate for the shortcomings of PTT and inhibit local recurrence.¹⁷ Although chemo-photothermal therapy can seemingly maximize the inhibition of tumor recurrence in situ, while facing distant metastasis, it can still fail to induce a prolonged anti-tumor effect, thus less effective to prevent metastasis.

Fortunately, it was observed that the activities of various immune cells, their functions, and relevant pathways were significantly increased in TNBC patients,^{4,18,19} along with more tumor-infiltrating lymphocytes and a higher positive rate of programmed death ligand-1 (PD-L1), suggesting that immune checkpoint blockade (ICB) would potentially promote anti-tumor therapy and prevent metastasis.^{20–22} ICB therapy uses anti-programmed cell death 1 (PD-1) and its ligand (PD-L1) antibodies to block the immune escape of cancer cells, ultimately inhibiting tumor metastasis and improving anti-tumor efficacy.^{23–25} Although promising, ICB alone presents a low objective response due to the inherent low immunogenicity.²⁶

When tumor cells die after undergoing certain therapeutics (eg, chemotherapy, PTT, radiotherapy), the accompanying transformation from non-immunogenic to immunogenic and mediating anti-tumor immune response is called immunogenic cell death (ICD).²⁷ During the ICD, the dying tumor cells produce a series of signaling molecules called damage-associated molecular patterns (DAMPs), mainly including the transfer of calreticulin (CRT) from the endoplasmic reticulum (ER) to the cell membrane surface, the release of high mobility group box 1 (HMGB1) protein from the nucleus, and the exocrine of adenosine triphosphate (ATP).^{28,29} These DAMPs will enhance the immunogenicity of cancer cells, initiating a series of cytological reactions, and ultimately activating innate and adaptive immune responses.^{30–33} Therefore, chemo-photothermal therapy is expected to trigger ICD,³⁴ and transfer the immunologically cold tumor to hot.³⁵ In combination with anti-PD-1 /PD-L1, tumor-infiltrating T cells can be significantly increased, thus achieving a lasting clinical response.^{15,36–38}

To achieve chemo-photothermal therapy, effective delivery of chemotherapeutic drugs and photothermal conversion agents to the tumor area is a prerequisite. Nanodrug delivery systems can improve the pharmacokinetics of drugs, enhance the ability of targeted delivery to tumors, accurately release drugs at the target site, and achieve better therapeutic effect while reducing side effects.^{39,40} Nanodrug delivery systems, such as liposomes, polymeric micelles, nanogels and biomimetic nanoparticles, have been widely used in the research of cancer therapy.^{39–41} As a typical representative of them, poly (lactic-co-glycolic acid) (PLGA) is one of the most successfully developed biocompatible and biodegradable polymers, and approved by US FDA.⁴² PLGA nanoparticles (NPs) are usually modified with poly ethylene glycol (PEG) for long blood circulation. The PEGylated PLGA polymer has been used as a carrier to encapsulate various small molecular drugs either hydrophobic or hydrophilic, large molecular proteins and enzymes, which can achieve the purpose of tumor combination therapy by loading different drugs.^{42,43} Given the limited inhibition of TNBC by monotherapy, combination therapy with multiple agents is essential. Therefore, PEGylated PLGA is a suitable drug delivery system candidate to achieve highly efficient TNBC therapy.

Herein, we constructed a multifunctional nanoplatform by loading photosensitizers IR780 and a first-line chemotherapeutic drug DOX on PLGA-PEG NPs (designated as IDNPs), which can achieve chemo-photothermal therapy to eliminate a primary tumor (Scheme 1). IR780 is a fluorescent dye with great photothermal conversion capability and photoacoustic (PA)/fluorescence imaging performance, which can be utilized to induce PTT, as well as monitor the distribution of nanoplatforms and determine the optimal treatment time window. Assisted by IR780, these IDNPs could preferentially accumulate into 4T1 TNBC cells without additional other conjunctions and potentiate the therapeutic efficacy. ICD triggered by chemo-photothermal therapy will combine with ICB antibodies to efficiently inhibit the growth of distant tumors. This study provided an effective therapeutic modality to combat TNBC and distant metastasis, showing great promise.



Scheme 1 Scheme of the therapeutic mechanism. Guided by PA and fluorescence imaging, IDNPs accumulate in the tumor site and achieve chemo-photothermal therapy to eliminate a primary tumor upon laser irradiation. ICD triggered by chemo-photothermal therapy will combine with ICB antibodies to efficiently inhibit the growth of distant tumors.

Materials and Methods

Materials

PLGA (MW:20000, 50:50)-PEG (MW: 2000) was purchased from Xi'an Ruixi Biotechnology Co., Ltd (Xi'an, China). IR780 iodide and Poly (vinyl alcohol) (PVA) were obtained from Sigma-Aldrich (USA). Doxorubicin hydrochloride (DOX·HCl) was produced by Dalian Meilun Biotechnology Co., Ltd (Dalian, China). Dichloromethane (CH_2Cl_2) and isopropanol were purchased from Chongqing Chuandong Chemical Co., Ltd (Chongqing, China). Cell Counting Kit-8 (CCK-8), Calcein AM, and propidium iodide (PI) were purchased from Dojindo (Japan). HMGB1 antibody, CRT antibody, and FITC-conjugated secondary antibody were obtained from Proteintech Group, Inc. (Wuhan, China). ATP-enhanced kit was obtained from Beyotime Biotechnology Co., Ltd. (Shanghai, China). HMGB1, IFN- γ , and TNF- α ELISA Kits were purchased from JingMei Biotechnology Co., Ltd (Shenzhen, China). All chemical agents were used without further purification.

Fabrication of IDNPs

IDNPs were fabricated by a modified double emulsification method.⁴⁴ First, 50 mg of PLGA-PEG and 2 mg of IR780 were dissolved into 2 mL CH_2Cl_2 . Then, 10 mg DOX·HCl (dissolved in 200 μL deionized water) was added to the same

CH₂Cl₂ solution. The above mixture was subjected to a probe ultrasound sonication (75 W, 3 min). After that, 5% PVA salt solution was added to the emulsion. Afterward, lower ultrasonic power (60 W, 2.5 min) was applied to obtain the double emulsion. The prepared double emulsion was then mixed with 1% PVA salt solution followed by stirring for 4 h. After centrifugation (5000 rpm/min and 11,000 rpm/min for 10 min, respectively), the slurry was obtained. PLGA-IR780 (INPs) and PLGA-DOX (DNPs) were prepared following same procedures by removing DOX or IR780.

Characterization of IDNPs

The morphology of IDNPs were observed by transmission electron microscopy (TEM) and scanning electron microscopy (SEM). The size distribution and zeta potential were measured by a Malvern Mastersizer analyzer (Malvern Instruments Ltd., Malvern, UK). Ultraviolet–Visible (UV–vis) absorption spectra of PLGA, DNPs, INPs, IDNPs, different concentration of free DOX and free IR780 were obtained on an UV–vis spectrophotometer (SHIMADZU UV-2550, Japan). IDNPs were diluted to an appropriate concentration to measure their absorption for calculating the entrapment efficiency of DOX and IR780 in IDNPs, respectively. To assess the photothermal conversion performance, different concentrations (IR780 concentration: 0, 0.04, 0.08, 0.12, 0.16 and 0.20 mg/mL) of IDNPs suspension were added into the 96-well plate and irradiated with a NIR laser with an intensity of 1.5 W/cm² for 5 min. The temperature changes were recorded by an infrared imager.

Cell Culture and Animal Models

Murine breast cancer 4T1 cell lines were purchased from Wuhan Procell Life Technology Co., Ltd (Wuhan, China). Female Balb/c mice (6–8 weeks) were purchased from Hunan STA Laboratory Animal Co., Ltd, and raised in the Experimental Animal Center of Chongqing Medical University. Murine breast cancer 4T1 cells a logarithmic growth phase (1×10^6 cells) dispersed in PBS were injected into the breast pad on the left and right sides of each mouse to simulate the primary and distant tumors on days 10 and 7 before the treatment, respectively. Tumor volume was calculated as $\pi/6 \times \text{length} \times \text{width}^2$. All the animal experiments were approved by the Animal Ethics Committee of the First Affiliated Hospital of Chongqing Medical University (No. 2021-716). All procedures were conducted in accordance with the Institutional Animal Care and Use Committee of Chongqing Medical University.

Intracellular Uptake of IDNPs and in vitro Chemo-Photothermal Therapy

To determine the uptake of IDNPs by 4T1 cells, the cells were seeded on cell climbing slices for fluorescence microscopic observation or in 6-well plates for flow cytometry analysis, with a seeding density of 2×10^4 cells per slice and 1×10^4 cells per well, respectively. After overnight, DNPs and IDNPs suspensions (PLGA concentration: 0.15 mg/mL) were added. After 1, 2, 3, 4, 5, and 6 h of coinubation, the cells were observed by fluorescence microscopy (excitation wavelength: 561 nm) or analyzed by flow cytometry (excitation wavelength: 565 nm).

To investigate in vitro chemo-photothermal therapeutic efficacy, cells were divided into 6 groups, including the control group, laser group, DNPs group, IDNPs group, INPs + laser group, and IDNPs + laser group. Cells were seeded in 96-well plates with a density of 10^4 per well in 100 μ L complete culture medium. After overnight culture, 100 μ L of the above NPs were added to the corresponding wells. After 6 h of incubation, groups with laser irradiation were subjected to NIR laser irradiation (808 nm, 1.5 W/cm², 5 min). After another 1 h of incubation, the cell viability was measured by a CCK-8 assay. In addition, cells cultured in confocal dishes after various treatments were stained with Calcein-AM/PI to distinguish the living (red fluorescence) dead (green fluorescence) cells in the dish, and observed by confocal laser scanning microscopy (CLSM).

Biosafety Assay, PA Imaging, and Biodistribution of IDNPs

Healthy Balb/c mice (n = 5) were randomly divided into 5 groups (Control, 1st day, 3rd day, 7th day and 14th day), and intravenously injected with IDNPs suspension (10 mg/mL, 200 μ L). Mice without any treatments were set as the control. After 1, 3, 7 and 14 days of the injection, the blood routine of those mice were tested, the serum in each group was collected for liver and kidney function examination, and major organs were collected for H&E staining.

In vitro and in vivo PA imaging of IDNPs were performed on a Vevo LAZR Photoacoustic Imaging System (Visual Sonics Inc., Canada). PA images of IDNPs at different concentrations (PLGA concentration: 2, 4, 6, 8, 10 mg/mL) were

obtained and the corresponding PA intensities were measured. Tumor-bearing mice were injected intravenously with IDNPs (PLGA concentration: 5 mg/mL, 200 μ L), and PA images of the tumors were acquired at different time points (before the injection, and 1, 2, 4, 6, 24 and 48 h after the injection). The PA intensities were also measured. The biodistribution of IDNPs was tested by fluorescence imaging with In Vivo Imaging System and Living Image software (NightOWL II LB983, Berthold Technologies GmbH & Co.KG, Germany). Fluorescence images were obtained at different time points, which were consistent with that of PA imaging. After 48 h of the administration, tumors and major organs, including heart, liver, spleen, lung, and kidney, were excised for ex vivo fluorescence imaging to further monitor the distribution of IDNPs.

In vivo Chemo-Photothermal Therapy

For in vivo chemo-photothermal therapy, thirty Balb/c tumor-bearing mice were randomly divided into six groups ($n = 5$), including control group, laser group, DNPs group, IDNPs group, INPs + laser group, and IDNPs + laser group. The mice were intravenously injected with the corresponding NPs every three days (PLGA concentration: 5 mg/mL, 200 μ L). After 24 h of the injection, all the groups with laser irradiation were subjected to NIR laser irradiation (808 nm, 1.5 W/cm², 10 min). The temperature changes in the tumor tissues were recorded by an infrared thermal imager. To understand the tumor growth inhibition of each treatment, after 7 days, tumors were collected for hematoxylin-eosin (H&E) staining, proliferating cell nuclear antigen (PCNA) and terminal deoxynucleotidyl transferase dUTP Nick-End Labeling (TUNEL) fluorescence staining. The morphological changes and proliferation status of mouse breast cancer cells after treatment were recorded. We also observed the long-term survival conditions of each mouse, which are presented by tumor size.

ICD Examination

To evaluate the capability of ICD triggered by chemo-photothermal therapy, characteristics of DAMPs presented by dying cells, including the exposure of CRT, the release of HMGB1 from the nucleus, and exocrine ATP, were tested. For in vitro ICD examination, cells were seeded in 48-well plates, divided into six groups, and received various treatments as mentioned in [Intracellular Uptake of IDNPs and in vitro Chemo-Photothermal Therapy](#). Then, the culture media supernatants were collected for HMGB1 and ATP release detection by HMGB1 ELISA kit, ATP assay kit and BCA protein concentration assay kit, respectively. The adherent cells were then stained with HMGB1 antibody, CRT antibody, and the corresponding secondary antibodies for fluorescence microscope and CLSM observation. For in vivo ICD test, tumor-bearing mice were divided and received the corresponding treatments same as mentioned in [In vivo Chemo-Photothermal Therapy](#). After 7 days of the first treatments, the serum of the mouse was taken for HMGB1 ELISA detection, and the tumor tissues (5 in each group) of the mice were dissected for CRT and HMGB1 immunofluorescence staining, and the determination of ATP concentration.

Combination of Chemo-Photothermal Therapy-Triggered ICD and Anti-PD-1 for Enhanced Immunotherapy

To evaluate the therapeutic effect of chemo-photothermal therapy-triggered ICD and anti-PD-1, mice with bilateral tumors were randomly divided into control group, anti-PD-1 group, IDNPs + laser group, and IDNPs + laser + anti-PD-1 group. NPs were intravenously injected every three days (PLGA concentration: 5 mg/mL, 200 μ L). NIR laser were performed on the first tumors 24 h after the injection of the NPs. Anti-PD-1 were intravenously injected 48 h after the injection of the NPs. Part of the mice in different groups were euthanized after 1 day and 7 days of the treatments, and the serum of mice were collected to determine tumor necrosis factor- α (TNF- α) and interferon- γ (IFN- γ) by the corresponding ELISA kits. The distant tumors were dissected to prepare single cell suspensions, and stained with APC-CD3, FITC-CD45, and PE-CD8a for flow cytometry analysis. The tumors, body weights and survival status of mice were monitored.

Statistical Analysis

All data in this study was expressed as the mean \pm standard error. Statistical analysis was performed using the OriginPro 2022 software (OriginLab Corporation, Northampton, Massachusetts, USA). One-way analysis of variance (ANOVA)

followed by a least significant difference multiple comparison test was used to determine the statistical significance for multiple comparisons, and Student's *t*-test was used for the comparisons of two groups. $P < 0.05$ was considered as statistically significant. The standard symbols were presented as * $p < 0.05$, ** $p < 0.01$ and *** $p < 0.001$.

Results and Discussion

Synthesis and Characterization of IDNPs

PLGA, an FDA-approved biodegradable polymer, was used to encapsulate two cargoes, a NIR dye IR780 and a first-line chemotherapeutic drug DOX, by an optimized double emulsification method (Figure 1a).⁴⁴ As revealed by the TEM (Figure 1b) and SEM image (Figure 1c), the obtained IDNPs presented a well-defined spherical structure and homogeneous sizes. The size distribution and zeta potential of the NPs play an important role in their interaction with cancer cells, and their accumulation in the tumor during the blood circulation.⁴⁵ In this study, PEGylated PLGA was used for more drug delivery efficiency according to previous reports.^{43,46} The average hydrodynamic diameter as measured by DLS was approximately 243.87 nm (Figure 1d), which renders these IDNPs more likely to pass through the tumor leaky blood vessels and accumulate in tumor tissue, relying on the well-known enhanced permeation and retention (EPR) effect.⁴⁷ The negative zeta potential of -6.25 mV of IDNPs (Figure 1e) would also be beneficial for the accumulation, as negatively charged NPs are known to be more stable during blood circulation.^{48,49} By recording the adsorption spectrum of IR780, DOX and drugs-loaded PLGA NPs, (Figure 1f-h) respectively, it is seen that IDNPs exhibited obvious peaks both near 780 nm and 480 nm, which could be corrected to IR780 and DOX, respectively, demonstrating the successful encapsulation of the two cargoes. By recording the absorbance of IR780 and DOX (Figure S1), the loading efficacies of IR780 and DOX were calculated to be 83.44% and 5.98%, respectively. IR780, a typical NIR dye, has been reported to be an effective photothermal conversion reagent.⁵⁰ In this study, IR780-encapsulated IDNPs are expected to mediate

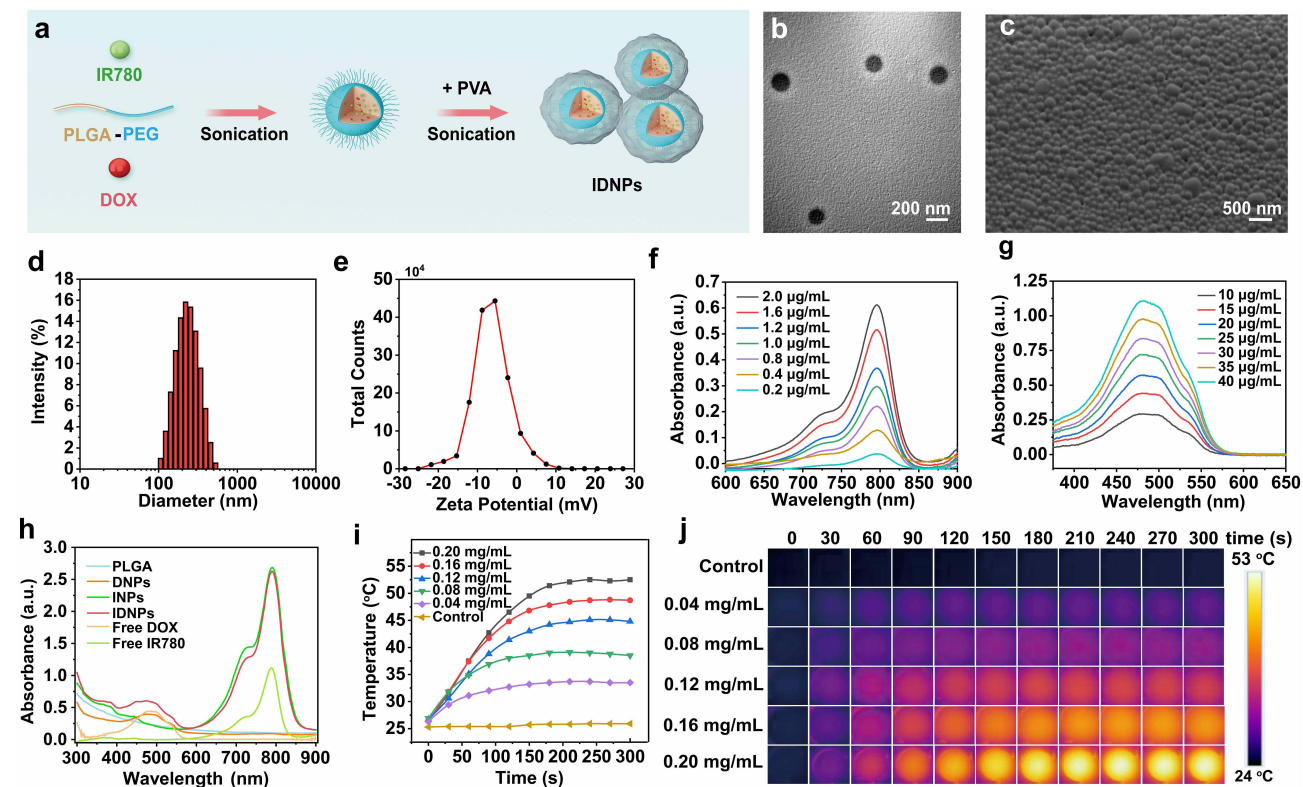


Figure 1 Characterization of IDNPs. (a) Schematic illustration of the synthesis of IDNPs. (b) TEM image of IDNPs. (c) SEM image of IDNPs. (d) Size distribution of IDNPs. (e) Zeta potential of IDNPs. (f) UV-vis absorbance spectra of IR780 at elevated concentration. (g) UV-vis absorbance spectra of DOX at elevated concentration. (h) Absorbance spectra of PLGA, DPNs, INPs, IDNPs, free DOX and free IR780. (i and j) Temperature changes of IDNPs at different IR780 concentrations under 808 nm laser irradiation (1.5 W/cm^2) and the corresponding thermal images.

PTT. The photothermal performance of IDNPs was evaluated *in vitro*. IDNPs at varied IR780 concentrations were exposed to an 808 nm laser. As shown in [Figure 1i](#) and [j](#), the temperature of the suspension could exceed to 50 °C within 5 min irradiation at the IR780 concentration of 0.20 mg/mL, which preliminarily indicated that IDNPs could be a prospective candidate for PTT against tumor cells/tissue.

Intracellular Uptake of IDNPs and *in vitro* Chemo-Photothermal Therapy

Efficient intracellular uptake is essential for both PTT and chemotherapy. Therefore, the uptake of IDNPs was assessed by fluorescence microscope and quantified by flow cytometry. As shown in [Figure 2a](#), red fluorescence in the images increased with prolonged incubation time in both DNPs and IDNPs treated groups. The nanoscaled size, negative zeta potential, and PEGylated may favor the cellular uptake.⁴³ However, cells internalized significantly more IDNPs than DNPs. This difference could be ascribed to IR780 loading in IDNPs, which is in accordance with previous reports.⁵⁰ Studies have demonstrated that IR780, a heptamethine indocyanine dye, could preferentially accumulate in certain types of tumor cells and act as a potential drug delivery agent. Although the targeting mechanism of such action remains to be elucidated, it may be related to organic anion transporter peptides (OATPs), which is known to mediate the transmembrane uptake of small molecule drugs and include structurally related fluorophores.^{51–53} The intracellular uptake efficacy of DNPs and IDNPs was compared by the fluorescence shift of DOX. From [Figure 2b](#), we found that the fluorescence in the IDNPs group is significantly enhanced compared with the DNPs group at the same time of incubation. The results of flow cytometry for intracellular uptake were consistent with that of CLSM observation.

Motivated by the efficient intracellular uptake and satisfactory photothermal performance, *in vitro* therapeutic efficacy of IDNPs was investigated next. Compared with the control group, chemotherapy with DOX-loaded DNPs presented a certain degree of cell-killing effect, with 72.76% cell viability ([Figure 2c](#)). When IR780 was integrated, the cell viability decreased to 51.84%, which should be ascribed to the efficient uptake mediated by IR780. Cells treated with INPs + laser (PTT-treated group) showed apparent cytotoxicity with 23.99% cell viability. Notably, the treatment of IDNPs + laser, the combination of PTT and chemotherapy, induced the strongest cytotoxicity, with significantly lower viability than other groups. Without the addition of IDNPs, the laser only showed neglectable cell-killing ability due to the lack of photothermal conversion agents. The combinational therapeutic effect of PTT and chemotherapy was also analyzed by flow cytometry, the trend of which was consistent with that of the CCK-8 results ([Figure 2e](#)). Additionally, cells after various treatments were co-stained with CAM and PI to distinguish dead cells (red) and live cells (green). As shown in [Figure 2d](#), there were only few dead cells in the group of laser only, demonstrating the relative safety of laser irradiation. In comparison, a substantial number of dead cells were observed in the IDNPs + laser treated group, which was consistent with the results of CCK-8, further supporting the robust therapeutic efficacy.

Biosafety Assay, PA Imaging, and Biodistribution of IDNPs

Before *in vivo* applications, the potential systemic toxicity of IDNPs was assessed after intravenous injection of IDNPs into mice by collection of blood samples and major organs for hematological assessment and H&E staining, respectively. The results of whole blood cell count, liver function indexes and kidney function indexes presents negligible differences in different stages (0, 1, 3, 7, 14 day) ([Figure 3a](#)). Meanwhile, the H&E staining analysis also showed no obvious physiological abnormality ([Figure 3b](#)). As a result, it is convinced the prepared-IDNPs showed prominent biosafety and biocompatibility *in vivo*.

With the increasing demand for precise treatment, diverse therapeutic nanoagents which are integrated with imaging capabilities to monitor the distribution of these nanoagents and determine the optimal therapeutic time-window, thereby improving the therapeutic effect. The integration of IR780 endowed these IDNPs with PA and fluorescence imaging performance. The PA imaging capability enhanced by IDNPs was evaluated. As shown in [Figure 4a](#), PA signals enhanced with the concentration of IDNPs. PA images were acquired after the administration of IDNPs *in vivo*. PA signals within tumor regions gradually increased, peaked at 24 h post-injection, and then decreased ([Figure 4b](#) and [c](#)). Furthermore, the biodistribution of IDNPs was assessed by fluorescence imaging. After intravenous administration of IDNPs, obvious fluorescence signals were observed in the tumor tissues at 1 h post-injection ([Figure 4d](#)). The signals within tumors gradually enhanced and peaked at 24 h post-injection ([Figure 4e](#)), which was consistent with the results of PA imaging.

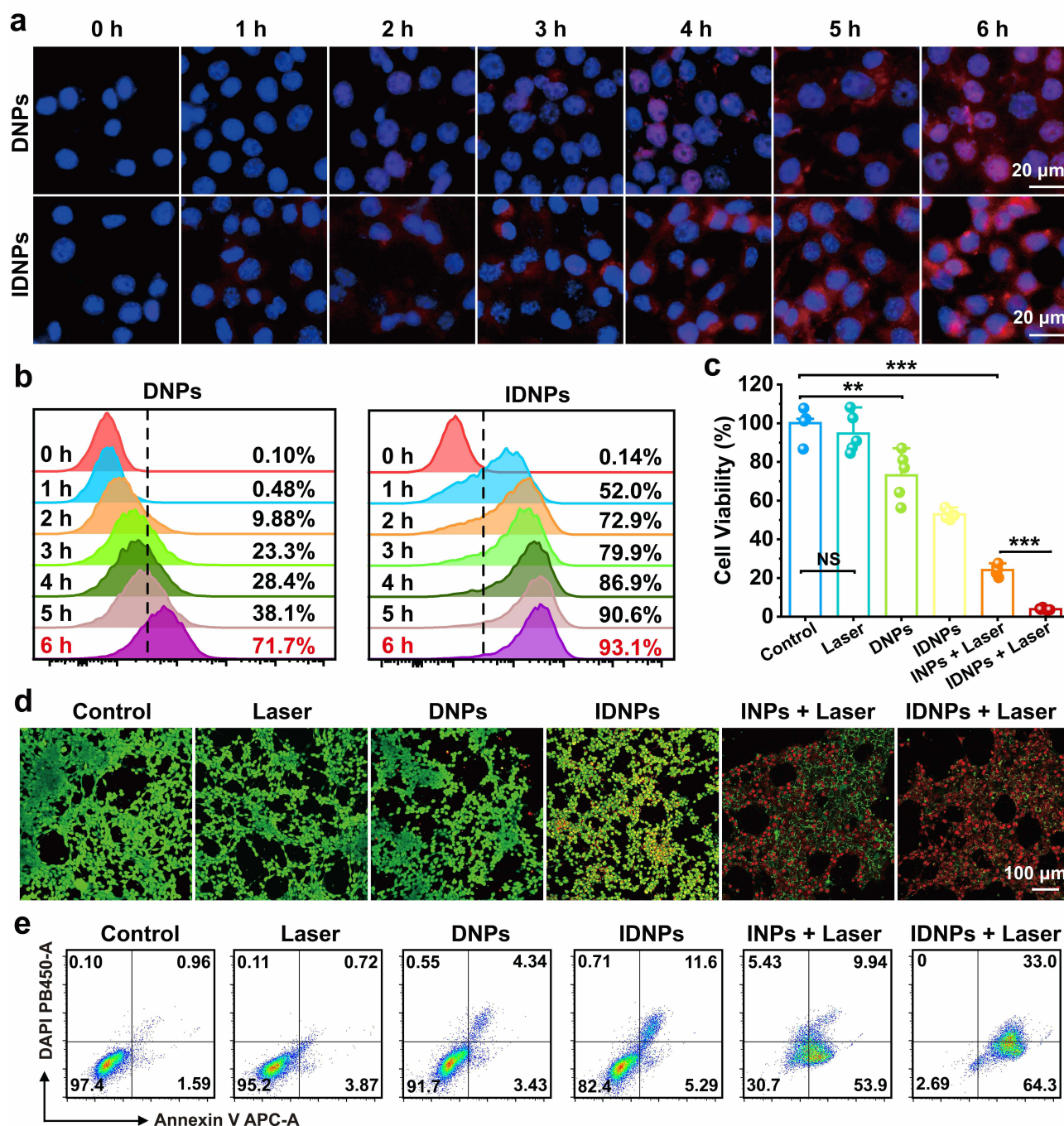


Figure 2 Intracellular uptake of IDNPs and in vitro chemo-photothermal therapy. (a) Intracellular uptake of DNPs and IDNPs as observed by fluorescence microscope after various intervals of incubation. (b) Flow cytometry analysis of intracellular uptake of DNPs and IDNPs after various intervals of incubation. (c) Relative cell viability of cells after different treatments ($n = 5$). (d) CLSM images of 4T1 cells costained with CAM and PI after various treatments. (e) Flow cytometry results for 4T1 cells apoptosis after various treatments. Data are represented as the mean \pm S.E.M. ** $P < 0.01$; *** $P < 0.001$.
Abbreviation: NS, not significant.

In addition, tumors and major organs, including heart, liver, spleen, lung, and kidney, were excised for ex vivo fluorescence imaging at 48 h post-injection. It was observed that fluorescence intensity of tumors was significantly higher than that of other organs (Figure 4f and g), indicating the preferential accumulation of these IDNPs in tumor tissues, which was beneficial for the following treatment. The satisfactory accumulation should also be associated with the negative zeta potential, and PEGylated PLGA NPs.⁴³

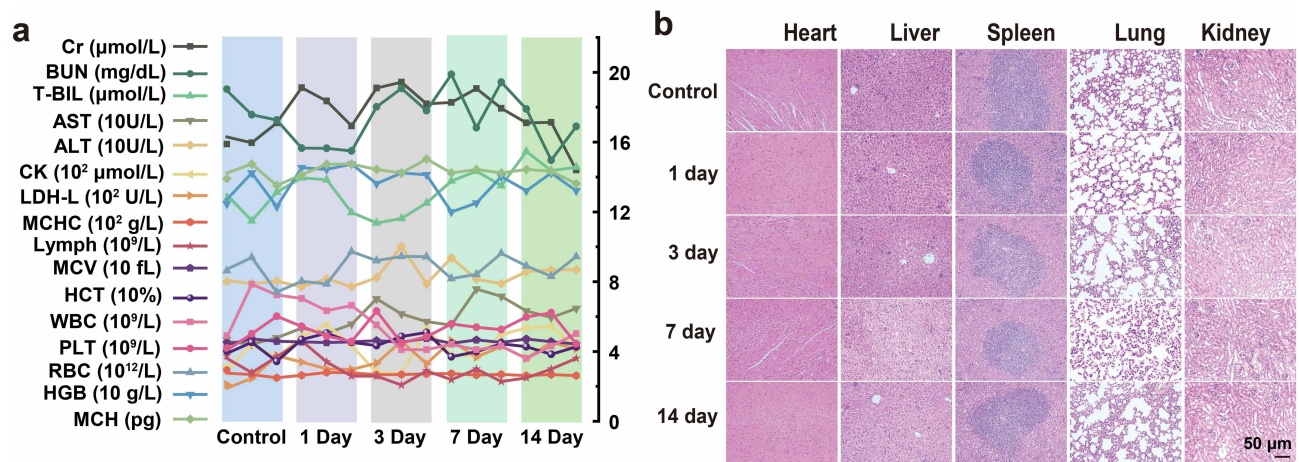


Figure 3 Biosafety assay of IDNPs. (a) Hematological and blood biochemical test of mice after intravenous administration of IDNPs at different time points. (b) H&E staining of major organs.

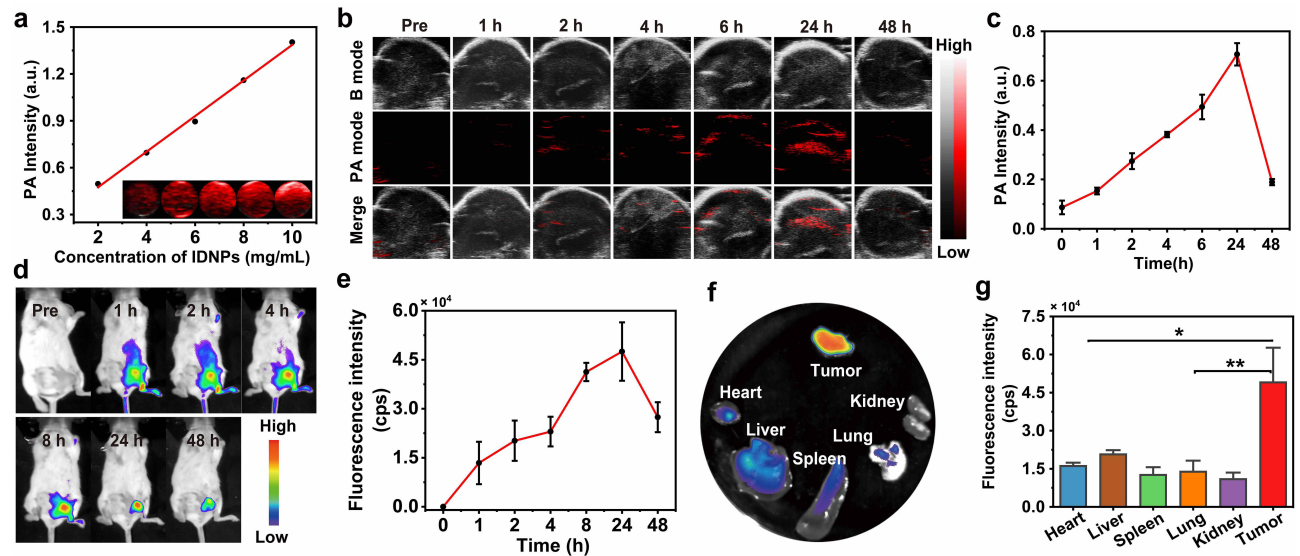


Figure 4 PA imaging, and biodistribution of IDNPs. (a) In vitro PA images and PA intensity of IDNPs at different concentrations. (b and c) In vivo PA images and PA intensity of tumors before and after intravenous injection of IDNPs at different time points. (d and e) In vivo fluorescence images of 4T1 tumor-bearing mice and fluorescence intensity of tumor after intravenous injection of IDNPs at different time points. (f and g) Ex vivo fluorescence images and fluorescence intensity of major organs and tumor dissected from mice 48 h post-injection of IDNPs. Data are represented as the mean \pm S.E.M. * $P < 0.05$; ** $P < 0.01$.

In vivo Chemo-Photothermal Therapy

Encouraged by the highly efficient chemo-photothermal therapy against tumor cells and desirable tumor accumulation in the aforementioned experiments, IDNPs were expected to demonstrate therapeutic efficacy in vivo. Tumor-bearing mice were randomly divided into 6 groups ($n = 5$), including control group, laser group, DNPs group, IDNPs group, INPs + laser group and IDNPs + laser group. According to the results of PA imaging and fluorescence imaging/ biodistribution, where IDNPs peaked at 24 h post-injection, this time point was hence selected for laser irradiation. A schematic of these treatment modalities was illustrated in Figure 5a. Upon laser irradiation, the temperature of the tumors in groups of INPs and IDNPs containing IR780 increased rapidly and exceeded 50 °C, which was sufficient to ablate tumors (Figure 5b and c).

In the groups of INPs + laser and IDNPs + laser, the tumors were ablated after twice of laser irradiation, and obvious scabs were observed in the tumor regions 24 h after the treatments. Scabs gradually became smaller with prolonged

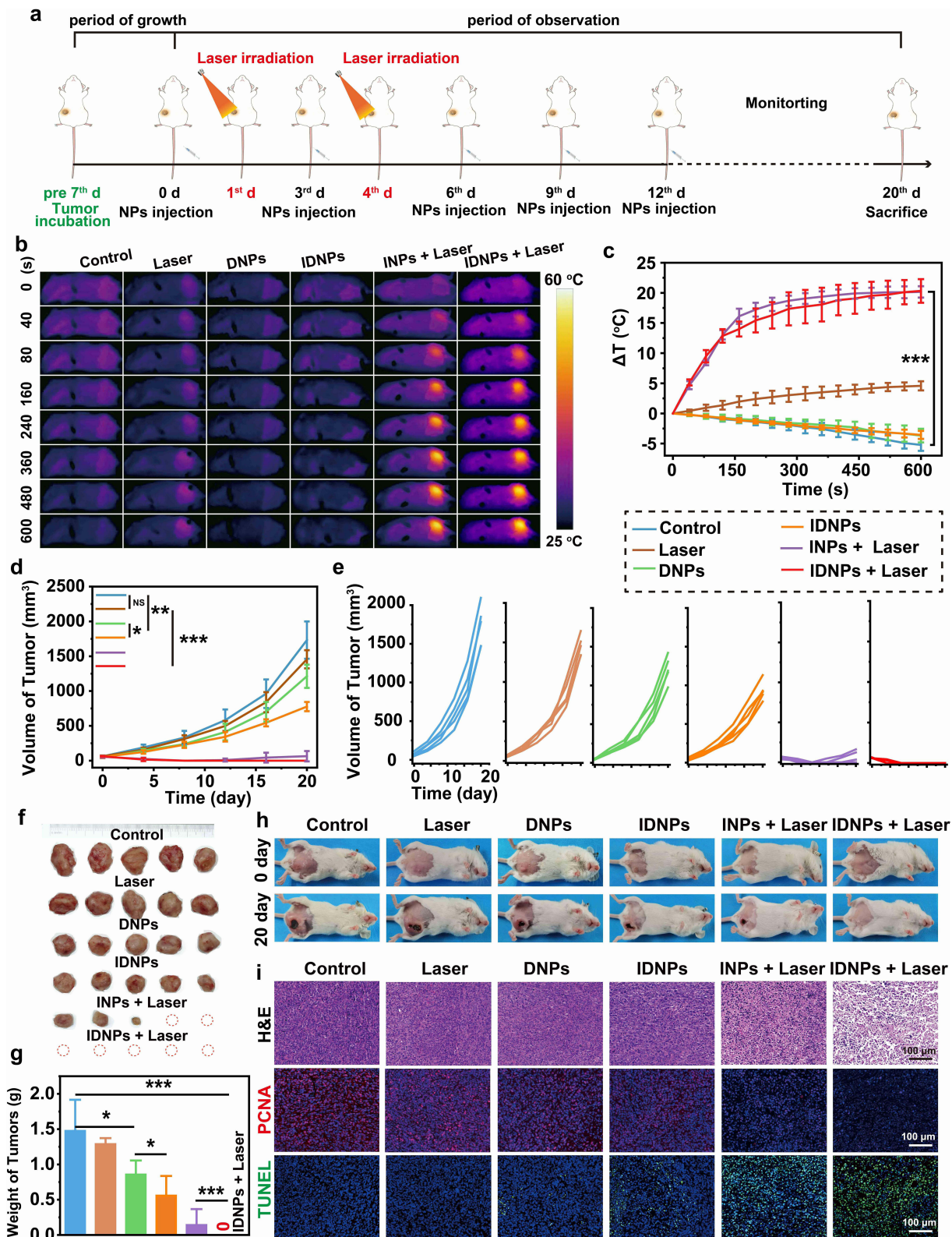


Figure 5 In vivo chemo-photothermal therapy. (a) Schematic illustration of IDNPs for primary tumors. (b and c) The corresponding IR thermal images and temperature changes at tumor regions of the six groups. (d and e) Tumor volume changes of six groups after various treatments (n = 5). (f) Photographs of tumors dissected from mice of six groups after various treatments. (g) Weight of tumors after 20 days of various treatments (n = 5). (h) Photographs of mice of six groups on day 0 and day 20 of treatment. (i) H&E/PCNA/TUNEL staining of tumor sections after various treatments. Data are represented as the mean ± S.E.M. *P < 0.05; **P < 0.01; ***P < 0.001. **Abbreviation:** NS, not significant.

observation time. However, recurrences were observed in 3 mice of the INPs + laser (PTT) group on the 12th, 16th, and 20th days, respectively (Figure 5d–f). Tumors treated by IDNPs + laser, which integrated both PTT and chemotherapy, were completely ablated without visible recurrence, which should be ascribed to the chemotherapeutic effect. Consistent with the results of the *in vitro* treatment, DNPs presented slight tumor inhibition (25.45-fold increase compared with the original volume) in comparison with the control group (28.12-fold increase), and the IDNPs showed a much better inhibitory effect (14.53-fold increase) than DNPs. While PTT may not completely ablate all tumor cells due to the limited penetration depth of the laser, DOX could be a reinforcement to make up for the blind area of NIR laser irradiation, and effectively inhibit the potential recurrence. In addition, only a negligible inhibitory effect was observed in the laser only-treated group, showing that NIR laser irradiation would not influence tissues without nanoagents, which demonstrated the safety of laser irradiation.

To further evaluate the therapeutic outcome, tumors were dissected and sliced for pathological examination (Figure 5i). H&E staining showed that the tumor nucleus had undergone nuclear lysis in the IDNPs + laser group, and the proportion of nuclear lysis was significantly higher than that in the other groups, indicating that the IDNPs + laser group had the most significant killing effect on tumor tissue. Similarly, in TUNEL (red fluorescence) fluorescence images, substantial necrosis (red fluorescence) was observed in the IDNPs + laser group. The expression of PCNA (red fluorescence), a kind of DNA polymerase accessory proteins, reflects the proliferation activity of cells. The tendency of red fluorescence in PCNA was opposite to that in TUNEL, and the IDNPs + laser group presented a significantly lower rate of cell proliferation. The results of the histological examination indicated an efficient therapeutic outcome of chemo-photothermal therapy.

ICD Examination

Although we have demonstrated that IDNPs-based chemo-photothermal therapy are highly efficient in combating primary tumor without obvious recurrence, the distant metastases remain intractable. Fortunately, it has been extensively reported that dying cancer cells induced by PTT or chemotherapy would release tumor antigens, and trigger systemic immune responses to fight against distant metastases, which is known as ICD. To investigate the ICD potentially induced by IDNP-based chemo-photothermal therapy, DAMPs-related biomarkers, including HMGB1, CRT, and ATP, were systematically investigated both *in vitro* and *in vivo*.

For *in vitro* ICD examination, after various treatments as listed in [Materials and Methods](#), cells were stained with anti-CRT for immunofluorescence observation, and culture supernatant was collected to test the release of HMGB1 and the section of ATP by the corresponding kits. CLSM observation in [Figure 6a](#) showed that IDNPs and IDNPs + laser induced CRT on tumor cells. In comparison, the chemo-photothermal therapy, IDNPs + laser significantly promoted the exposure of CRT, which act as a “eat me” signal and facilitate the uptake of apoptotic cells by phagocytes. HMGB1 is a highly conserved nuclear protein, which can be released specifically in response to certain cellular damages. As shown in [Figure 6b](#) and [c](#), both chemotherapy and PTT could trigger the release of HMGB1. The HMGB1 levels increased by 1.43-fold, 1.54-fold and 1.59-fold, in IDNPs, INPs + laser group and IDNPs + laser groups, respectively, which was consistent with the cell damage degree shown in [Figure 2c](#). Dying cells also secrete ATP, providing a “find me” signal to recruit immune cells. The results ([Figure 6d](#)) showed ATP level increased by 4.39-fold after IDNPs treatment, by 8.72-fold after INPs + laser treatment, and by 15.61-fold after IDNPs + laser treatment, respectively. *In vivo* ICD was also investigated by measuring CRT exposure ([Figure 6e](#)), the release of HMGB1 ([Figure 6f](#) and [g](#)), and the section of ATP ([Figure 6h](#)) after 1 days of various treatments. The results were consistent with the *in vitro* results. Collectively, IDNPs can successfully induce ICD after NIR irradiation, improve the immunogenicity of the tumor, and transform breast cancer from “cold” to “hot” for activating antitumor immune response.

Combination of Chemo-Photothermal Therapy-Triggered ICD and Anti-PD-1 for Enhanced Immunotherapy

To investigate the potent potency of chemo-photothermal therapy-triggered ICD in combination with anti-PD-1 ICB immunotherapy in eliciting immune response and treating distant tumors, four groups of mice ($n = 3$) with bilateral tumors were utilized and treated as follows: (i) control groups with saline injection; (ii) anti-PD-1 injection (intraperitoneal injection, *i.p.*); (iii) IDNPs + laser irradiation, chemo-photothermal therapy; (iv) IDNPs + laser + anti-PD-1,

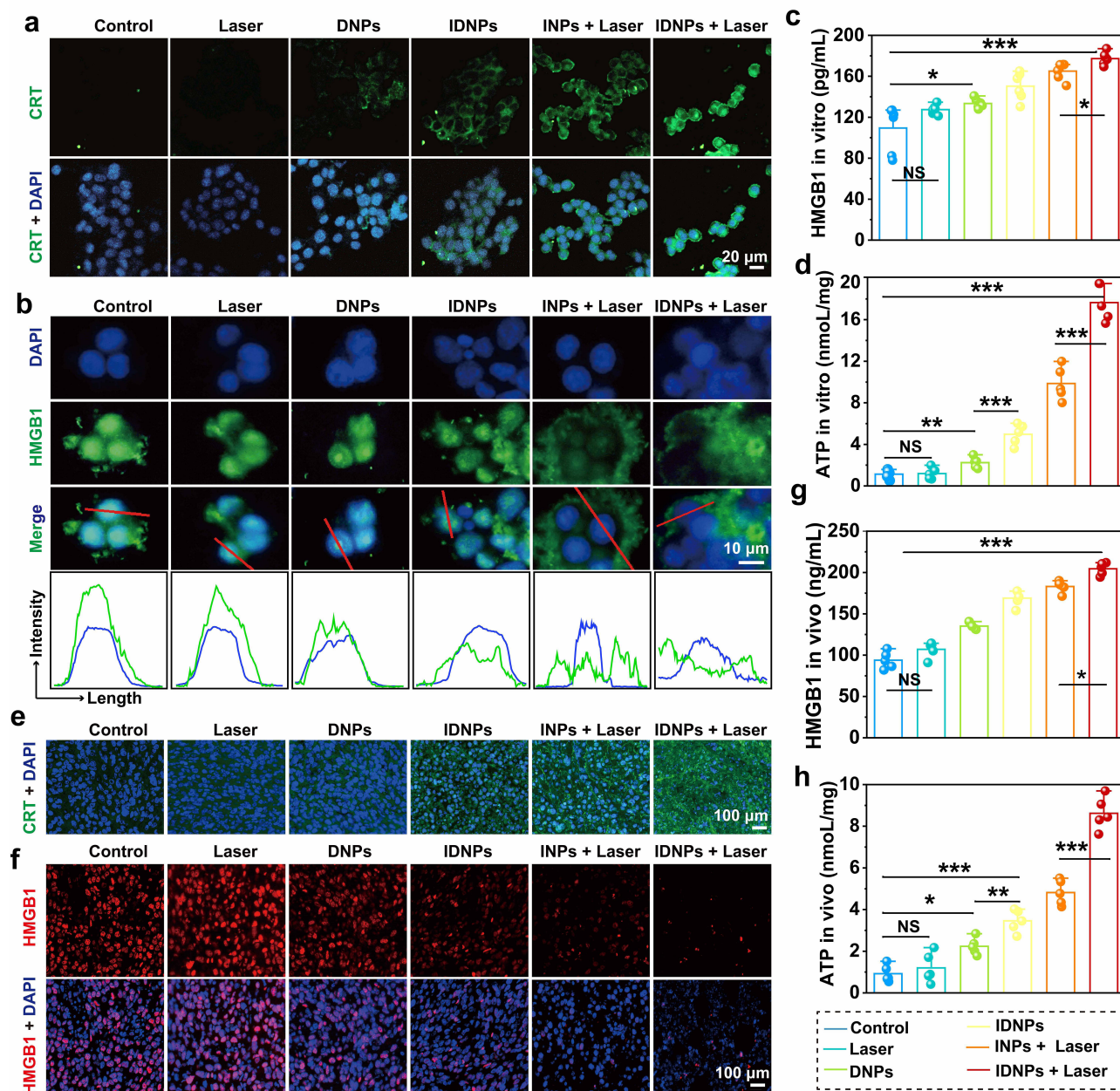


Figure 6 ICD examination. (a) The express of CRT in vitro after different treatments as observed by CLSM. (b) The release of HMGB1 in vitro after different treatments were observed by fluorescence microscope. (c) The release of HMGB1 in vitro after different treatments as measured by ELISA (n = 5). (d) The release of ATP in vitro after different treatments as measured by ELISA (n = 5). (e and f) The express of CRT and HMGB1 in vivo after different treatments as measured by ELISA (n = 5). (g and h) The release of HMGB1 and ATP in vivo after different treatments as measured by ELISA (n = 5). Data are represented as the mean ± S.E.M. *P < 0.05; **P < 0.01; ***P < 0.001. Abbreviation: NS, not significant.

Abbreviation: NS, not significant.

chemo-photothermal therapy + ICB. A schematic was illustrated in Figure 7a. CD8⁺ T lymphocytes, the main effector cells, play a dominant role in cancer immunotherapy, and can attack cancer cells by releasing perforin and other effector molecules. On the 7th day after various treatments, distant tumors were dissected, and made into single-cell suspensions were prepared to analyze the population of tumor-infiltrating CD8⁺ T cells. As shown in Figure 7b and c, the combination of chemo-photothermal therapy and anti-PD-1 ICB therapy could significantly improve the proportion of CD8⁺ T cells (CD45⁺CD3⁺CD8⁺) in distant tumors, with a ratio of 8.65 ± 1.26%, respectively. However, anti-PD-1 ICB monotherapy and chemo-photothermal therapy-triggered ICD slightly elevated the proportion of CD8⁺ T cells in distant tumors. In addition to intratumoral CD8⁺ T cells analysis, serum cytokines including IFN-γ and TNF-α, which are biomarkers

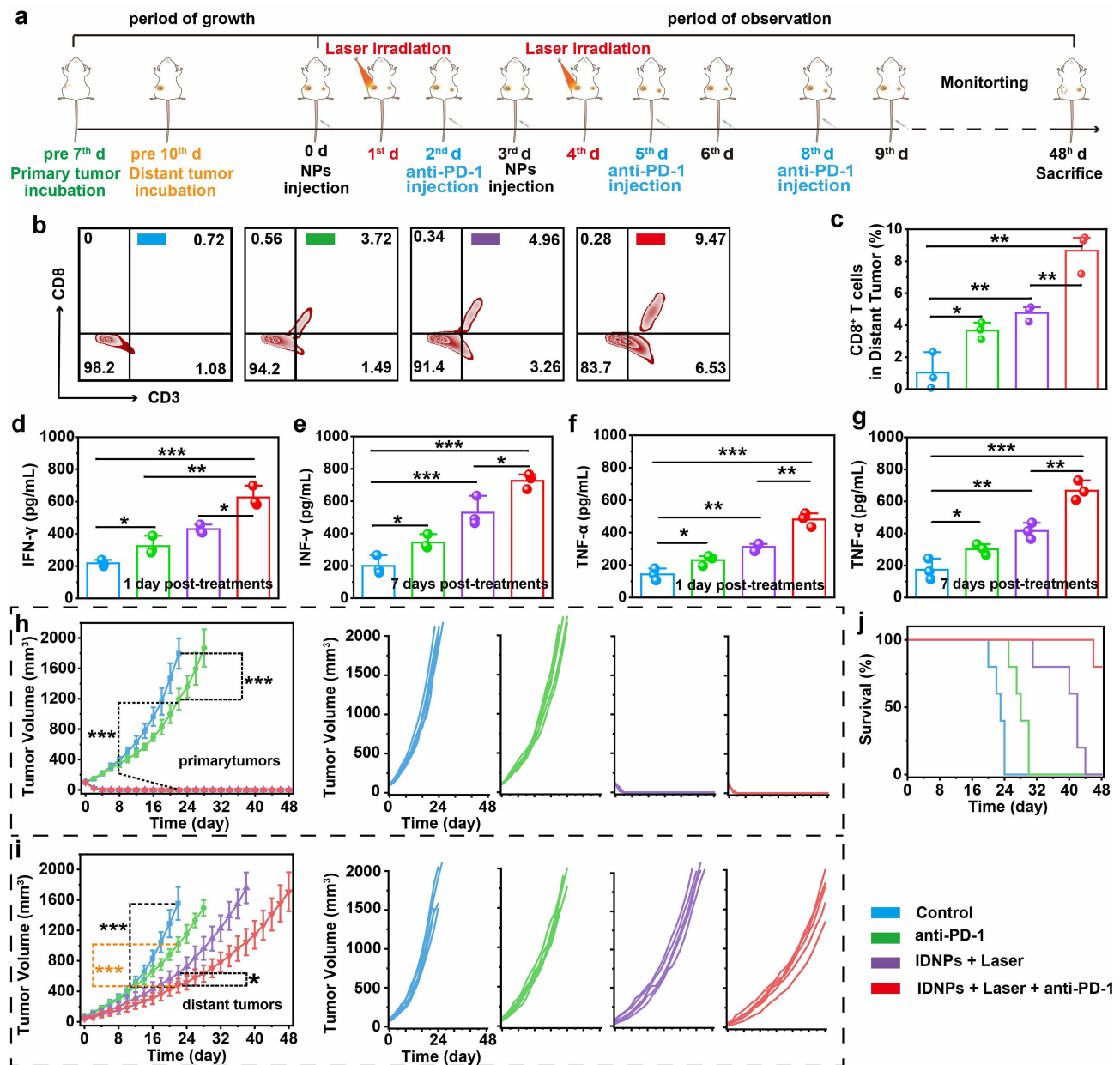


Figure 7 Combination of chemo-photothermal therapy-triggered ICD and Anti-PD-1 for enhanced immunotherapy. (a) Schematic diagram of combining IDNPs with anti-PD-1 strategy for inhibiting distant tumors. (b and c) Flow cytometry analysis of CD8⁺ T cells in distant tumors after various treatments (n = 3). (d and e) IFN-γ in serum at 1 day and 7 days after various treatments as measured by ELISA (n = 3). (f and g) TNF-α in serum at 1 day and 7 days after various treatments as measured (n = 3). (h) Tumor volume changes of the primary tumors after various treatments (n = 5). (i) Tumor volume changes of the distant tumors after various treatments. (j) Survival curve of mice in each group (n = 5). Data are represented as the mean ± S.E.M. *P < 0.05; **P < 0.01; ***P < 0.001.

released by immune cells, were also evaluated at 1 day and 7 days after various treatments (Figure 7d–g). ELISA results showed that 1 day after the treatments, the content of IFN-γ in mice treated with ICD + anti-PD-1 (625.93 ± 63.82 pg/mL) was significantly higher than those mice treated with anti-PD-1 only (324.16 ± 56.17 pg/mL). Consistent with IFN-γ results, 1 day after different treatments, it was found that the secretion of TNF-α in mice treated with ICD + anti-PD-1 (467.72 ± 64.24 pg/mL) was also higher than in mice that received the anti-PD-1 injection (230.30 ± 31.31 pg/mL). Additionally, the secretion of both IFN-γ and TNF-α showed the same tendency at 7 days post various treatments. The combination of ICD and anti-PD-1 showed the highest serum IFN-γ and TNF-α content, and the difference was statistically significant compared with other groups. Together, these results suggested IDNPs-mediated chemo-

photothermal immunotherapy synergized the vaccination effect with the ICD triggered by chemo-photothermal therapy, stimulating superior systemic immune responses over mono-treatment.

Based on the potent systemic immune response, we next evaluated the tumor inhibitory effect of the combination of ICD and anti-PD-1 on both primary and distant tumors. As expected, chemo-photothermal therapy indeed suppressed the growth of distant primary tumors, but the inhibitory effects on were not desirable. And mono anti-PD-1 ICB therapy only slightly inhibit the tumor growth whether primary tumor or distant tumors, which contributed to poor tumor immunogenicity. When combined with chemo-photothermal therapy-triggered ICD, the distant tumors were significantly inhibited as compared to the mono anti-PD-1 ICB therapy and ICD (Figure 7h and i). It is noteworthy that the median survival time of mice with combinational treatment was determined to be 48 days, significantly longer than 27 and 28 days for mice treated with anti-PD-1 and chemo-photothermal therapy, respectively (Figure 7j). These findings demonstrated that antitumor immunotherapy was remarkably strengthened in combination with ICD and anti-PD-1 ICB therapy. In addition, negligible fluctuation in the body weight of mice in various groups was observed during the observation period, indicating the safety of these interventions (Figure S2).

Conclusion

In summary, multifunctional IDNPs were successfully synthesized to mediate chemo-photothermal therapy to combat primary TNBC and trigger ICD, eventually inhibiting the growth of distant tumors in combination with ICB antibodies. Characterization results indicated a successful loading of both IR780 and DOX, with loading efficiencies of 83.44% and 5.98%, respectively. Efficient intracellular uptake and tumoral accumulation of IDNPs have been demonstrated, which would essentially be contributing to the remarkable therapeutic effect. In the presence of laser irradiation, cell viability dropped to 2.53% compared with the control group. Biodistribution and efficient tumoral accumulation of IDNPs were monitored by PA/fluorescence imaging. In vivo evaluation suggested that upon NIR laser irradiation, IDNPs induced highly efficient chemo-photothermal therapeutic effect against primary tumors. More importantly, chemo-photothermal therapy triggered ICD, which combined with anti-PD-1 provoked a systemic antitumor immune response against distant tumors. This study provided valuable information both preclinically and clinically.

Abbreviations

ICD, immunogenic cell death; PTT, Photothermal therapy; DOX, Doxorubicin; CTA, cancer therapy agent; ROS, reactive oxygen species; ER, endoplasmic reticulum; CTL, cytotoxic T cells; DC, dendritic cells; IL-2, interleukin-2; IL-4, interleukin-4; INF- γ , interferon- γ ; CRT, calreticulin; HMGB1, high mobility group box 1; ATP, adenosine triphosphate; PD-1, programmed cell death 1; TNBC, Triple negative breast cancer; PR, progesterone receptor.

Acknowledgments

This work was supported by the National Natural Science Foundation of China (No. 82171949), Chongqing Natural Science Foundation key project (No. cstc2019jcyj-zdxmX0019), and Chongqing Postgraduate Scientific Research and Innovation project (No. CYB21166).

Disclosure

The authors report no conflicts of interest in this work.

References

1. Sung H, Ferlay J, Siegel RL, et al. Global cancer statistics 2020: GLOBOCAN estimates of incidence and mortality worldwide for 36 cancers in 185 countries. *CA Cancer J Clin.* 2021;71(3):209–249. doi:10.3322/caac.21660
2. Zhu Y, Zhu X, Tang C, Guan X, Zhang W. Progress and challenges of immunotherapy in triple-negative breast cancer. *Biochim Biophys Acta Rev Cancer.* 2021;1876(2):188593. doi:10.1016/j.bbcan.2021.188593
3. Jiang YZ, Ma D, Suo C, et al. Genomic and transcriptomic landscape of triple-negative breast cancers: subtypes and treatment strategies. *Cancer Cell.* 2019;35(3):428–440 e425. doi:10.1016/j.ccell.2019.02.001
4. Bianchini G, De Angelis C, Licata L, Gianni L. Treatment landscape of triple-negative breast cancer-expanded options, evolving needs. *Nat Rev Clin Oncol.* 2022;19(2):91–113. doi:10.1038/s41571-021-00565-2

5. Alamdari SG, Amini M, Jalilzadeh N, et al. Recent advances in nanoparticle-based photothermal therapy for breast cancer. *J Control Release*. 2022;349:269–303. doi:10.1016/j.jconrel.2022.06.050
6. Yang F, Xiao Y, Ding J-H. Ferroptosis heterogeneity in triple-negative breast cancer reveals an innovative immunotherapy combination strategy. *Cell Metab*. 2023;35(1):84–100.e108. doi:10.1016/j.cmet.2022.09.021
7. Keenan TE, Tolaney SM. Role of immunotherapy in triple-negative breast cancer. *J Natl Compr Canc Netw*. 2020;18(4):479–489. doi:10.6004/jnccn.2020.7554
8. Pradipta AR, Tanei T, Morimoto K, Shimazu K, Noguchi S, Tanaka K. Emerging technologies for real-time intraoperative margin assessment in future breast-conserving surgery. *Adv Sci*. 2020;7(9):1901519. doi:10.1002/advs.201901519
9. Ahmad SS, Crittenden MR, Tran PT. Clinical development of novel drug-radiotherapy combinations. *Clin Cancer Res*. 2019;25(5):1455–1461. doi:10.1158/1078-0432.Ccr-18-2466
10. Zetner D, Kamby C, Gülen S. Quality-of-life outcomes following topical melatonin application against acute radiation dermatitis in patients with early breast cancer: a double-blind, randomized, placebo-controlled trial. *J Pineal Res*. 2023;74(1):e12840. doi:10.1111/jpi.12840
11. Nel J, Elkhoury K, Velot E, et al. Functionalized liposomes for targeted breast cancer drug delivery. *Bioact Mater*. 2023;24:401–437. doi:10.1016/j.bioactmat.2022.12.027
12. Zhen X, Pu K, Jiang X. Photoacoustic imaging and photothermal therapy of semiconducting polymer nanoparticles: signal amplification and second near-infrared construction. *Small*. 2021;17(6):e2004723. doi:10.1002/smll.202004723
13. Sun Y, Lyu B, Yang C. An enzyme-responsive and transformable PD-L1 blocking peptide-photosensitizer conjugate enables efficient photothermal immunotherapy for breast cancer. *Bioact Mater*. 2023;22:47–59. doi:10.1016/j.bioactmat.2022.08.020
14. Li X, Lovell JF, Yoon J, Chen X. Clinical development and potential of photothermal and photodynamic therapies for cancer. *Nat Rev Clin Oncol*. 2020;17(11):657–674. doi:10.1038/s41571-020-0410-2
15. Xie Z, Fan T, An J, et al. Emerging combination strategies with phototherapy in cancer nanomedicine. *Chem Soc Rev*. 2020;49(22):8065–8087. doi:10.1039/d0cs00215a
16. Cheng Y, Chen Q, Qian Z. Versatile red blood cells for triple-negative breast cancer treatment via stepwise photoactivations. *Adv Healthc Mater*. 2023;12(3):e2201690. doi:10.1002/adhm.202201690
17. Huang X, Zha F, Zou J, Li Y, Wang F, Chen X. Photoacoustic imaging-guided synergistic photothermal/radiotherapy using plasmonic Bi/Bi₂O₃-x nanoparticles. *Adv Funct Mater*. 2022;32(23):2113353. doi:10.1002/adfm.202113353
18. Liu Z, Jiang Z, Gao Y, Wang L, Chen C, Wang X. TP53 mutations promote immunogenic activity in breast cancer. *J Oncol*. 2019;2019:5952836. doi:10.1155/2019/5952836
19. Baldominos P, Barbera-Mourelle A, Barreiro O. Quiescent cancer cells resist T cell attack by forming an immunosuppressive niche. *Cell*. 2022;185(10):1694–1708.e1619. doi:10.1016/j.cell.2022.03.033
20. Voorwerk L, Slagter M, Horlings HM, et al. Immune induction strategies in metastatic triple-negative breast cancer to enhance the sensitivity to PD-1 blockade: the TONIC trial. *Nat Med*. 2019;25(6):920–928. doi:10.1038/s41591-019-0432-4
21. Maharjan R, Choi JU, Kweon S. A novel oral metronomic chemotherapy provokes tumor specific immunity resulting in colon cancer eradication in combination with anti-PD-1 therapy. *Biomaterials*. 2022;281:121334. doi:10.1016/j.biomaterials.2021.121334
22. Killock D. Chemotherapy as a TONIC to invigorate PD-1 inhibition in TNBC. *Nat Rev Clin Oncol*. 2019;16(8):464. doi:10.1038/s41571-019-0232-2
23. Konstantinidou M, Zarganes-Tzitzikas T, Magiera-Mularz K, Holak TA, Domling A. Immune checkpoint PD-1/PD-L1: is there life beyond antibodies? *Angew Chem Int Ed Engl*. 2018;57(18):4840–4848. doi:10.1002/anie.201710407
24. Cristescu R, Mogg R, Ayers M, et al. Pan-tumor genomic biomarkers for PD-1 checkpoint blockade-based immunotherapy. *Science*. 2018;362:6411. doi:10.1126/science.aar3593
25. Xiao B-L, Wang X-L, Xia H-F. HRS regulates small extracellular vesicle PD-L1 secretion and is associated with anti-PD-1 treatment efficacy. *Cancer Immunol Res*. 2023;11(2):228–240. doi:10.1158/2326-6066.Cir-22-0277
26. Blomberg OS, Spagnuolo L, Garner H. IL-5-producing CD4⁺ T cells and eosinophils cooperate to enhance response to immune checkpoint blockade in breast cancer. *Cancer Cell*. 2023;41(1):106–123.e110. doi:10.1016/j.ccell.2022.11.014
27. Li W, Yang J, Luo L, et al. Targeting photodynamic and photothermal therapy to the endoplasmic reticulum enhances immunogenic cancer cell death. *Nat Commun*. 2019;10(1):3349. doi:10.1038/s41467-019-11269-8
28. Hayashi K, Nikolos F, Lee YC, et al. Tipping the immunostimulatory and inhibitory DAMP balance to harness immunogenic cell death. *Nat Commun*. 2020;11(1):6299. doi:10.1038/s41467-020-19970-9
29. Zhang S, Wang J, Kong Z, et al. Emerging photodynamic nanotherapeutics for inducing immunogenic cell death and potentiating cancer immunotherapy. *Biomaterials*. 2022;282:121433. doi:10.1016/j.biomaterials.2022.121433
30. Li L, Tian H, Zhang Z. Carrier-free nanoplatform via evoking pyroptosis and immune response against breast cancer. *ACS Appl Mater Interfaces*. 2023;15(1):452–468. doi:10.1021/acsami.2c17579
31. Galluzzi L, Vitale I, Warren S, et al. Consensus guidelines for the definition, detection and interpretation of immunogenic cell death. *J Immunother Cancer*. 2020;8(1):e000337. doi:10.1136/jitc-2019-000337
32. Dai X, Shen L, Zhang J. Cold atmospheric plasma: redox homeostasis to treat cancers? *Trends Biotechnol*. 2023;41(1):15–18. doi:10.1016/j.tibtech.2022.07.007
33. Guo B, Qu Y, Sun Y. Co-delivery of gemcitabine and paclitaxel plus NanoCpG empowers chemioimmunotherapy of postoperative “cold” triple-negative breast cancer. *Bioact Mater*. 2023;25:61–72. doi:10.1016/j.bioactmat.2023.01.014
34. Yu Z, Guo J, Hu M, Gao Y, Huang L. Icaritin exacerbates mitophagy and synergizes with doxorubicin to induce immunogenic cell death in hepatocellular carcinoma. *ACS Nano*. 2020;14(4):4816–4828. doi:10.1021/acsnano.0c00708
35. Duan X, Chan C, Lin W. Nanoparticle-mediated immunogenic cell death enables and potentiates cancer immunotherapy. *Angew Chem Int Ed Engl*. 2019;58(3):670–680. doi:10.1002/anie.201804882
36. Banstola A, Poudel K, Kim JO, Jeong JH, Yook S. Recent progress in stimuli-responsive nanosystems for inducing immunogenic cell death. *J Control Release*. 2021;337:505–520. doi:10.1016/j.jconrel.2021.07.038
37. Heshmati Aghda N, Abdulsahib SM, Severson C, et al. Induction of immunogenic cell death of cancer cells through nanoparticle-mediated dual chemotherapy and photothermal therapy. *Int J Pharm*. 2020;589:119787. doi:10.1016/j.ijpharm.2020.119787

38. Xie L, Wang G, Sang W, et al. Phenolic immunogenic cell death nanoinducer for sensitizing tumor to PD-1 checkpoint blockade immunotherapy. *Biomaterials*. 2021;269:120638. doi:10.1016/j.biomaterials.2020.120638
39. Ye Q, Lin Y, Li R, Wang H, Dong C. Recent advances of nanodrug delivery system in the treatment of hematologic malignancies. *Semin Cancer Biol*. 2022;86(Pt 2):607–623. doi:10.1016/j.semcancer.2022.03.016
40. Cheng Z, Li M, Dey R, Chen Y. Nanomaterials for cancer therapy: current progress and perspectives. *J Hematol Oncol*. 2021;14(1):85. doi:10.1186/s13045-021-01096-0
41. Haggag YA, Yasser M, Tambuwala MM, El Tokhy SS, Isreb M, Donia AA. Repurposing of Guanabenz acetate by encapsulation into long-circulating nanopolymersomes for treatment of triple-negative breast cancer. *Int J Pharm*. 2021;600:120532. doi:10.1016/j.ijpharm.2021.120532
42. Danhier F, Ansorena E, Silva JM, Coco R, Le breton A, Préat V. PLGA-based nanoparticles: an overview of biomedical applications. *J Control Release*. 2012;161(2):505–522. doi:10.1016/j.jconrel.2012.01.043
43. Haggag Y, Elshikh M, El-Tanani M, Bannat IM, McCarron P, Tambuwala MM. Nanoencapsulation of sophorolipids in PEGylated poly(lactide-co-glycolide) as a novel approach to target colon carcinoma in the murine model. *Drug Deliv Transl Res*. 2020;10(5):1353–1366. doi:10.1007/s13346-020-00750-3
44. Gao C, Chen Y, Cheng X. A novel structurally identified epitope delivered by macrophage membrane-coated PLGA nanoparticles elicits protection against *Pseudomonas aeruginosa*. *J Nanobiotechnology*. 2022;20(1):532. doi:10.1186/s12951-022-01725-x
45. Blanco E, Shen H, Ferrari M. Principles of nanoparticle design for overcoming biological barriers to drug delivery. *Nat Biotechnol*. 2015;33(9):941–951. doi:10.1038/nbt.3330
46. Huang SJ, Wang TH, Chou YH, et al. Hybrid PEGylated chitosan/PLGA nanoparticles designed as pH-responsive vehicles to promote intracellular drug delivery and cancer chemotherapy. *Int J Biol Macromol*. 2022;210:565–578. doi:10.1016/j.ijbiomac.2022.04.209
47. Geng S, Guo M, Zhan G. NIR-triggered ligand-presenting nanocarriers for enhancing synergistic photothermal-chemotherapy. *J Control Release*. 2023;353:229–240. doi:10.1016/j.jconrel.2022.11.039
48. Du J-Z, Li H-J, Wang J. Tumor-acidity-cleavable maleic acid amide (TACMAA): a powerful tool for designing smart nanoparticles to overcome delivery barriers in cancer nanomedicine. *Acc Chem Res*. 2018;51(11):2848–2856. doi:10.1021/acs.accounts.8b00195
49. Wang J, Li Y, Nie G. Multifunctional biomolecule nanostructures for cancer therapy. *Nat Rev Mater*. 2021;6(9):766–783. doi:10.1038/s41578-021-00315-x
50. Li Y, Hu D, Pan M. Near-infrared light and redox dual-activatable nanosystems for synergistically cascaded cancer phototherapy with reduced skin photosensitization. *Biomaterials*. 2022;288:121700. doi:10.1016/j.biomaterials.2022.121700
51. Zhang E, Luo S, Tan X, Shi C. Mechanistic study of IR-780 dye as a potential tumor targeting and drug delivery agent. *Biomaterials*. 2014;35(2):771–778. doi:10.1016/j.biomaterials.2013.10.033
52. Nies AT, Schaeffeler E, Schwab M. Hepatic solute carrier transporters and drug therapy: regulation of expression and impact of genetic variation. *Pharmacol Ther*. 2022;238:108268. doi:10.1016/j.pharmthera.2022.108268
53. Yokomizo S, Henary M, Buabeng ER. Topical pH sensing NIR fluorophores for intraoperative imaging and surgery of disseminated ovarian cancer. *Adv Sci*. 2022;9(20):e2201416. doi:10.1002/advs.202201416

International Journal of Nanomedicine

Dovepress

Publish your work in this journal

The International Journal of Nanomedicine is an international, peer-reviewed journal focusing on the application of nanotechnology in diagnostics, therapeutics, and drug delivery systems throughout the biomedical field. This journal is indexed on PubMed Central, MedLine, CAS, SciSearch®, Current Contents®/Clinical Medicine, Journal Citation Reports/Science Edition, EMBase, Scopus and the Elsevier Bibliographic databases. The manuscript management system is completely online and includes a very quick and fair peer-review system, which is all easy to use. Visit <http://www.dovepress.com/testimonials.php> to read real quotes from published authors.

Submit your manuscript here: <https://www.dovepress.com/international-journal-of-nanomedicine-journal>